

# APPLICATION OF ATOMIC BEAMS FOR PLASMA DIAGNOSTIC

B. Schweer

Institut für Plasmaphysik, Forschungszentrum Jülich GmbH, EURATOM Association,  
Trilateral Euregio Cluster, 52425 Jülich, Germany, (49)2461-615536

## I. INTRODUCTION

Plasma can be studied and characterised by the analysis of its radiation<sup>1,2</sup>. Signals obtained by passive spectroscopy contain much information about temperature, density and flux of the main species and impurities<sup>3</sup>. The interpretation of measured line intensities requires the knowledge of atomic physics describing the specific radiation from the plasma. Tomographic methods are applied but they need symmetries for the calculation of local parameters. Additionally in magnetic confined plasmas the interpretation might be more difficult due to the Zeeman splitting.

Asymmetries and steep gradients of plasma parameters as it appears in the plasma boundary of a tokamak or stellarator require the direct local measurement of these quantities. There are two methods to probe the plasma locally, by a laser or an atomic beam. In both cases, elastic collisions lead to scattering of light (Thomson scattering<sup>4</sup>), respectively atoms (Rutherford scattering<sup>5</sup>) and inelastic collisions cause the emission of light that is analysed (laser induced fluorescence<sup>6</sup>, atomic beam diagnostics).

In this article we will concentrate on the interaction of beam atoms with plasma, yielding to optical emission, which is observed with spectroscopic methods. After interaction with the bulk plasma the beam atoms or deuterons and impurity ions can be investigated. The first method is called beam emission spectroscopy (BES), the second charge exchange recombination spectroscopy (CXRS).

Both techniques need two ports, one for the injection and a second for observation, which should be nearly perpendicular in order to get the best spatial resolution. The location of the measurement is determined by the intersection of the beam with the (perpendicular) line of sight of the detection system

This paper is structured in four chapters. After this introduction the basic properties of atomic beam injection used for BES and CXRS are described in chapter II. The collisional-radiative model necessary for the interpretation of the measured line intensities is presented in the third part. Examples of atomic beam sources applied in tokamaks and evaluated signals are given in the last chapter.

## II. BASICS FOR ATOMIC BEAM INJECTION

In magnetic confined plasmas only neutral atoms can enter the plasma where they interact usually with electrons

and ions. The beam atoms are first excited and then ionised. The corresponding emission profile increases to a maximum there the loss processes by ionisation dominate. The density of injected neutrals drops until all atoms are ionised. The penetration depth depends on the ionisation energy and on the velocity of the injected atoms. As an example the calculated emission profiles of thermal (500°C) Li, thermal (150°C) He and 5 eV (laser blow-off) Li, injected into a plasma with given  $n_e$  and  $T_e$  profiles, are compared in fig. 1. The ionisation energy of Li is 6.35eV and that of He is 24.9eV. Although the kinetic energy of He atoms is much smaller than that of the suprathermal Li they have comparable penetration depths.

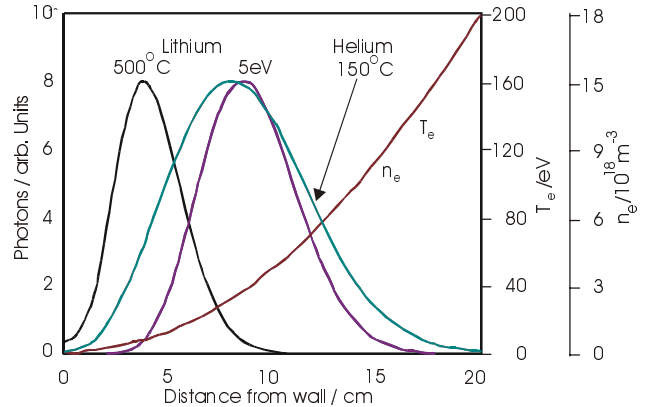


Figure 1: Comparison of penetration depths for thermal Li, thermal He and suprathermal Li

Different selection criteria have to be considered for the choice of atoms injected into the plasma:

### II.1. No disturbance of the plasma

If the injected atoms are volatile, e.g. for helium, accumulation effects during a discharge may lead to an increase of electron density and falsify the measurements. A He concentration of <10% of the ion density does not influence the plasma significantly. Condensing materials can cause other problems. They are accumulated at the first wall over long operation periods and can be released by plasma interaction. The radiation potential of high Z atoms can reduce significantly the plasma temperature and lead to instabilities. Therefore only low Z-materials like lithium and carbon are selected.

The kinetic energy of the injected atoms determines the interaction with electron and/or ions. At low energies, like for thermal beams only interaction with electrons has to be

considered. At high energies (keV) proton collisions and charge exchange processes dominate the excitation processes. The collision and radiation processes for excitation of the probing beam are strongly dependent on the initial population of the electronic states, which then also determines the penetration depth.

### II.2. Knowledge of atomic data

Atomic beam diagnostic relies strongly on the knowledge of atomic data. The cross-sections for collision of atoms with electrons and ions and the oscillator strengths for radiation processes must be known considerably. In fusion plasmas the operational range of the electron density does not allow the application of the corona equilibrium. In most cases a collisional-radiative model, which describes the excitation and de-excitation processes, must be applied.

The observation wavelength selected should have a large transition probability in order to reach high S/N ratios and better time resolutions.

Line radiation from the plasma can require the selection of transitions with lower oscillator strengths. In particular the background light, the so-called passive signal can be discriminated from the active by chopped particle beams. This affords larger dynamic ranges of the detection system in order to resolve the modulation depth. Figure 2 presents an example of a CXRS signal obtained with a dynamic range of 2024 counts (11bit) and a modulation depth of about 20% (50 counts), which was still sufficient for data evaluation.

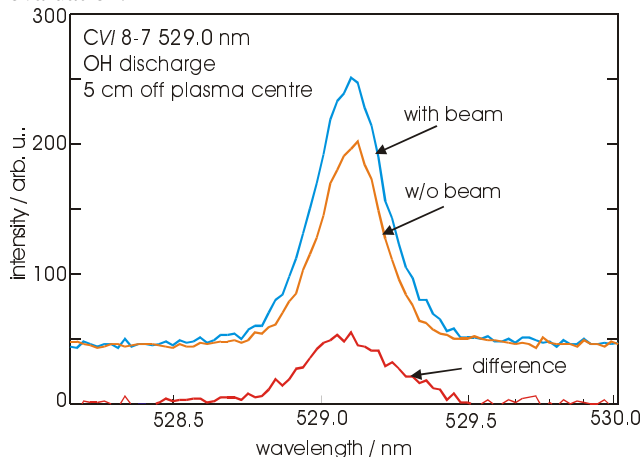


Figure 2: Discrimination of the active CXRS signal of CVI using a chopped H beam

Depending on the sensitivity range of the detector even lines with weaker oscillator strengths might be selected. Near the wall the selection of lines in the infrared spectra might be unfavourably influenced by continuum radiation from hot surfaces. Further the line splitting of the Zeeman effect induced by the strong magnetic fields in tokamaks increases with larger wavelengths, resulting in a more complicated (broaden) structure of the observed transition.

### II.3. Properties of Atomic Beam Sources

Atomic beams are produced by thermal sources, suprathermal sources, and neutralised accelerated ions. The selection of atomic beam sources depends on the beam divergence, the reliability, expenditure and costs.

#### II.3.a. Thermal sources

Thermal sources are easy to produce. Their energies are below 0.1 eV and they can deliver a high continuous particle flux, which can be modulated by mechanical choppers. Their disadvantage is the large divergence that only can be influenced by the introduction of apertures into the beam. Clearly thermal sources are the cheapest and most reliable beams if solid-state emitters are used. They have a large inventory and therefore they can be operated over long periods of time.

#### II.3.b. Suprathermal sources

Higher energies up to 10 eV are produced by laser blow-off technique. Thin films are deposited on glass or quartz substrates. Onto the rear side of the substrate a powerful laser beam is focussed. The material must absorb the radiation and then a plasma is produced. This plasma expands and very fast the main free path for collisions is so large that the energy is frozen to the ions. They can still capture an electron and penetrate with a sufficient low divergence of  $\pm 5^\circ$  into the probing plasma. This method allows only pulsed operation (100 $\mu$ s). The determination of the background light from the plasma is done before or after the cloud has passed the observation volume. Very high particle fluxes, pre-selected by the spot size, are achieved, but only condensing materials can be selected. Lasers with repetition rates up to 30 Hz are applied. High costs are produced by the powerful laser system and the target movement and control system.

#### II.3.c. Neutralised accelerated ions

A wide range of energy is covered by ion beams, which are accelerated by an applied voltage. The ion flux is dependent on the voltage and therefore a sufficient flux is only reached for energies above a few keV. In order to enter the tokamak plasma the ions must first be neutralised in a gas target by charge exchange. Depending on the element different conditions for the initial population can be established. Although this particle sources have beneficial low divergences ( $< \pm 1^\circ$ ) the particle density is quite low due to the high velocity. The emission signal, however, is proportional to the particle density. But for high electron densities only high-energy beams can penetrate sufficiently deep into the plasma.

The system needs an ion source, an ion optical system, deflection plates, a neutraliser and a strong vacuum pumping system. Therefore the costs are high. The reliability depends on the source type.

There are not only technical reasons for the selection of the beam source. For BES the product of velocity and relaxation time gives the spatial resolution of the measured quantity. The population of the excited levels is calculated by solving the time dependent differential equations of a

collisional-radiative model as a function of plasma parameter by Runge–Kutta methods. The injected atoms should reach an equilibrium determined by the ratio between the excited and ground level, which defines the relaxation time.

### III. COLLISIONAL RADIATIVE MODEL

Beam atoms entering the plasma will have interactions (inelastic scattering) with electrons and ion that lead to excitation and ionisation. These processes are dependent on the density and temperature of the plasma. The excitation of electrons causes radiative transitions that are observed. The interpretation of these signals is only possible if all interaction and transition processes are considered in a collisional-radiative model. The atomic data, rate coefficients, transition probabilities and lifetimes have to be known quite accurately in order to receive reliable results. The balance equation of the state  $i$  can be written as follows<sup>7</sup>

$$\begin{aligned} \frac{\partial}{\partial t} n_i = & + \sum_{j,j \neq i} \langle \sigma_{e,ji} v \rangle n_e n_j & - \sum_{j,j \neq i} \langle \sigma_{e,ij} v \rangle n_e n_i \\ & \text{gain by electron impact excitation} & \text{gain by electron loss excitation} \\ & + \sum_{j,j \neq i} \langle \sigma_{p,ji} v \rangle n_{ion} n_j & - \sum_{j,j \neq i} \langle \sigma_{p,ij} v \rangle n_{ion} n_i \\ & \text{gain by ion impact excitation} & \text{gain by ion loss excitation} \\ & + \sum_{j,j < i} A_{ji} n_j & - \sum_{j,j < i} A_{ij} n_i \\ & \text{gain by spontaneous emission} & \text{loss by spontaneous emission} \\ & & - \langle \sigma_{e \rightarrow ion,i} v \rangle n_e n_i \\ & & \text{loss by electron impact ionisation} \\ & & - \langle \sigma_{p \rightarrow ion,i} v \rangle n_{ion} n_i \\ & & \text{loss by ion impact ionisation} \\ & & - \langle \sigma_{cx,i} v \rangle n_{ion} n_i \\ & & \text{loss by charge exchange} \end{aligned}$$

$n_e, n_{ion}$  = density of electrons, resp. ions,  $n_i, n_j$  = population density of the states  $i$ , resp.  $j$ ,  $\langle \sigma_{e,ij} v \rangle, \langle \sigma_{p,ij} v \rangle$  = rate coefficients for electron, resp. ion impact excitation from state  $i$  to  $j$ ,  $A_{i,j}$  = transition probability for spontaneous emission from the state  $i$  to  $j$ ,  $\langle \sigma_{e \rightarrow ion,i} v \rangle, \langle \sigma_{p \rightarrow ion,i} v \rangle$  = rate coefficients for electron, resp. ion impact ionisation,  $\langle \sigma_{cx,i} v \rangle$  = rate coefficients for charge exchange

Fortunately for many applications this equation can be simplified. In table 1 for different energies the collision rates of ground state Li atoms with electrons and protons are compared. It can be seen that only for beam energies in the keV range proton collisions and charge exchange has to be considered:

process	Thermal	1 keV	10 keV
Excitation by e-collision $e+\text{Li}(2s) \rightarrow e+\text{Li}(2p)$	$8.0 \cdot 10^5/\text{s}$	$8.0 \cdot 10^5/\text{s}$	$8.0 \cdot 10^5/\text{s}$
Ionisation by e-collision $e+\text{Li}(2s) \rightarrow e+\text{Li}^+$	$9.0 \cdot 10^4/\text{s}$	$9.0 \cdot 10^4/\text{s}$	$9.0 \cdot 10^4/\text{s}$
Excitation by p-collision $p+\text{Li}(2s) \rightarrow p+\text{Li}(2p)$	$<10^4/\text{s}$	$1.5 \cdot 10^4/\text{s}$	$1.4 \cdot 10^5/\text{s}$
Ionisation by p-collision $p+\text{Li}(2s) \rightarrow p+\text{Li}^+$	$<10^4/\text{s}$	$\approx 2.0 \cdot 10^4/\text{s}$	$1.5 \cdot 10^5/\text{s}$
p-charge exchange $p+\text{Li}(2s) \rightarrow \text{H}+\text{Li}^+$	$<3 \cdot 10^3/\text{s}$	$5.0 \cdot 10^3/\text{s}$	$1.05 \cdot 10^5/\text{s}$

Table 1: Rates for electron and proton collisions with ground state Li and for charge exchange

#### III.1. Beam emission spectroscopy

In optical thin plasmas the intensity of line radiation is determined by the emission coefficient<sup>8</sup>.

$$\epsilon_{ij} = \frac{h\nu_{ij}}{4\pi} n_i A_{ij} \quad (1)$$

where  $n_i$  is the population density in the excited state  $i$  with Einstein coefficients  $A_{ij}$  for spontaneous emission into the state  $j$ . The energy of this transition is  $h\nu_{ij}$  with the frequency  $\nu_{ij}$ . The integration over the line of sight  $d\ell$  delivers the measured line intensity.

$$I = \int \frac{h\nu_{ij}}{4\pi} n_i A_{ij} d\ell \quad (2)$$

In most cases the population of the excited states is small compared to ground state  $n_1$  and therefore the density of the injected atoms  $n_{beam} \approx n_1$  and  $n_i \ll n_1$ . As a consequence higher states are only populated by (electron) collisions and depopulated mainly by radiative transitions in lower states. This means that loss processes by collisions can be neglected.

$$n_i A_{ij} \gg n_e n_i \langle \sigma v_e \rangle \quad (3)$$

The emission signal is dependent on the observation volume  $V$ , the local density of the beam atoms  $n_{beam}$ , the electron density  $n_e$ , and the excitation rate coefficient  $\langle \sigma v \rangle_e$  that is a function of temperature:

$$I_r \propto \sum_{k \neq j} \frac{A_{i \rightarrow j}}{A_{i \rightarrow k}} \int n_e(r,t) n_{beam}(r,t) \langle \sigma v \rangle_e V dt \quad (4)$$

The quantity in front of the integral represents the branching ratio. In this case the collisions with ions and charge exchange are not considered.

The local density of the beam atoms can be deduced from the emission profile of the observed line transition.

$$n_{beam}(r) = \int_0^r n_e(r') n_{beam}(r') \frac{\langle \sigma_{i,j} v_e \rangle}{\bar{v}} dr \quad (5)$$

where  $r$  is directed opposite to the beam direction and  $\bar{v}$  the mean velocity of the injected atoms.

Combining equation 4 and 5 (branching ratio=1) the electron density is dependent on:

$$n_e(r) = \frac{\bar{v}I(r)}{\langle \sigma_{ex} v_e \rangle \int_0^r \frac{\langle \sigma_l v_e \rangle}{\langle \sigma_{ex} v_e \rangle} I(r') dr'} \quad (6)$$

The electron density can be evaluated from the intensity if the  $T_e$  profile is known from another diagnostic or if the rate coefficients are only weakly dependent on the temperature and kept constant. This is the case for Li-atoms.

The temperature can be measured if a second element is injected into the plasma. Usually an element with a strong dependence of the rate coefficient on  $T_e$ , like carbon, is selected. The penetration depth of the second element should nearly cover that of the first element. This is the case for the combination of lithium and carbon.

The intensity profiles must be measured simultaneously. Equation 6 can be written for both elements and then  $n_e$  and  $T_e$  profiles can be calculated. The time resolution  $\Delta t$  for these measurements is strongly dependent on signal intensity. Of course the beam density must be below values that could disturb the plasma. The time resolution is also ruled by the relaxation time deduced from the collisional-radiative model.

The application of high energy neutralised ion beams for beam emission spectroscopy needs further information of the rate coefficients for the interaction with ions and for charge exchange.

A second method of beam emission spectroscopy is applied on He-beams. It is based on the fact that the temperature dependence of the rate coefficients in the singlet and in the triplet systems behaves different (fig. 3). Therefore it was proposed to measure  $T_e$  from the ratio of the line intensities. But the method failed. Brenning<sup>9</sup> found that different transfer processes have to be taken into account. In 1990 for He a complete set of atomic data<sup>10</sup> was calculated and the development of a collisional-radiative model<sup>11</sup> yields to reasonable explanation of the measured signals<sup>12</sup>. Meanwhile powerful models for the calculation of rate coefficients are established which have increased the reliability of  $n_e$  and  $T_e$  measurements<sup>13</sup>.

The calculated line intensity ratios used for the simultaneous measurement of the local electron density and temperature are shown in Fig. 4. The data represent the ratios for equilibrium conditions. The ratio of the transitions at 668nm ( $2^1P-3^1D$ ) and 728nm ( $2^1P-3^1S$ ) (dashed line) are most sensitive to  $n_e$  and weakly dependent on  $T_e$ . The inverse dependence is given for the ratio of the transitions at 728nm and 706nm ( $2^3P-3^3S$ ) (solid line), used for the determination of  $T_e$ . As can be seen in fig. 4 the curves of line intensity ratios are not orthogonal anymore for temperatures below 10 eV leading to an intolerable error. A lower limit for the measurement of the electron density is at  $< 2 \cdot 10^{18}/m^3$  where the relaxation time is too long and the typical decay lengths of the plasma parameters are shorter than the relaxation length. The penetration length of the

injected He-atoms, which are ionised by the plasma, settles the upper limit of the measurement.

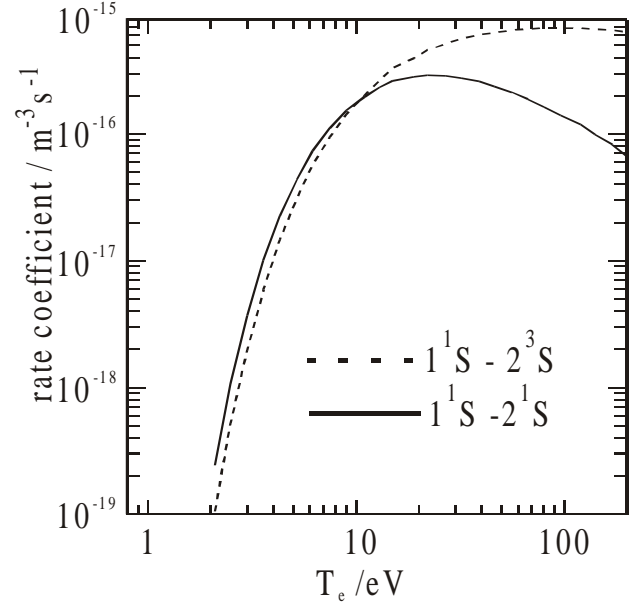


Figure 3: Rate coefficients in the singlet and triplet system of He

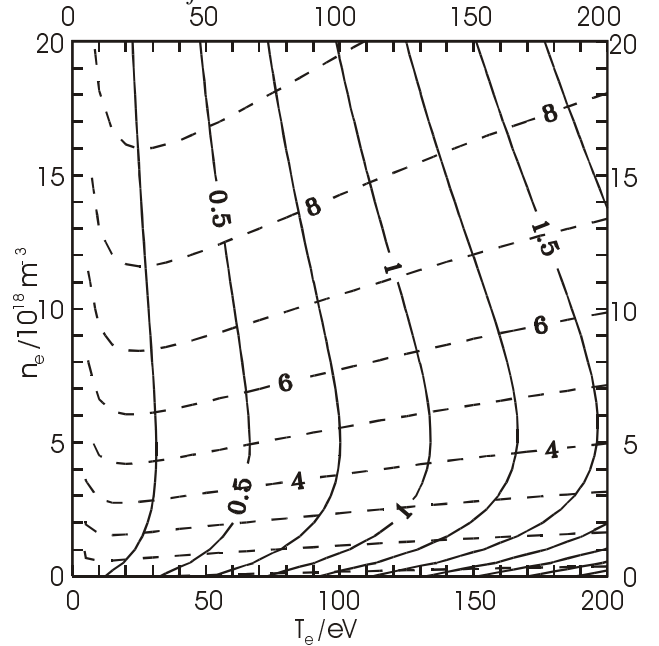


Figure 4 Calculated line intensity ratios of He for the determination of electron density and temperature

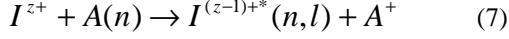
This diagnostic delivers local plasma parameters without knowing the history of beam penetration, e.g. the local density of He-atoms. The time resolution is directly connected to the relaxation time.

### III.2. Charge exchange recombination spectroscopy

In the previous section spectroscopic observation of the injected atoms were discussed. The plasma contains impurities that also will show characteristic radiation after inter-

action with beam atoms<sup>14</sup>. Due to the high temperatures in the core plasma of a tokamak electrons of light ions can be stripped completely. These ions cannot emit any line radiation. Therefore neutral atoms have to be injected which do charge exchange with the ions. The excited ions can radiate their characteristic line spectra when they decay to the ground level.

As a result of the reaction



an electron of the beam atom  $A(n)$  is captured by an impurity ion  $I^{z+}$  into an excited state with the quantum number  $n, \ell$ . The excited state then decays under emission of line radiation that is characteristic for the respective impurity. Usually the temperature is deduced from the Doppler broadening, the rotation velocity from the Doppler shift and the density of the impurities from the intensities of charge exchange recombination lines. The ion temperature,  $T_i$ , can be calculated from the spectral line width assuming a Maxwell distribution<sup>15</sup>

$$T_i = \frac{m_i}{k_B} \left( \frac{c \lambda_w}{\lambda_0 \sqrt{8 \ln 2}} \right)^2 \quad (8)$$

$m_i$  is the impurity mass,  $k_B$  Boltzmann's constant,  $c$  the speed of light,  $\lambda_w$  the full width at half maximum (FWHM) and  $\lambda_0$  the wavelength of the transition.

If the wavelength centre of the charge exchange recombination line is shifted in respect to an unperturbed line centre, the rotation velocity can be determined:

$$v_{rot} = c \frac{\Delta \lambda_{rot}}{\lambda_0} \quad (9)$$

The density of the impurity in the respective charge state,  $n_{z+}$  can be calculated if the emission cross-section  $\sigma_{em}$ , the local beam density  $n_{beam}$  and velocity  $v_{beam}$  are known.

$$\phi = \frac{1}{4\pi} \int n_{I^{z+}} n_{beam} \langle \sigma_{em} v_{beam} \rangle d\ell \quad (10)$$

In a magnetically confined plasma the interpretation of the charge exchange lines is much more complicated. Zeeman splitting and  $\ell$ -level mixing can produce a complex line structure and the intensity of the components is dependent on the direction of observation in respect to the magnetic field. These non-thermal effects broaden the CXRS line that usually still can be fitted by a Gaussian profile but the apparent ion temperature must be multiplied by a correction factor smaller than 1. The components of the fine structure splitting of the transition are distributed asymmetrically in respect to the theoretical central line. As a consequence velocity measurements must be corrected by an offset of the line centre. Additionally the halo (for H-beams) and luke warm effect can made complex line spectra<sup>16</sup>. The fitting procedure is always done with a multi Gaussian function assuming thermal Maxwellian distributions.

The halo effect is caused by charge exchange of neutral hydrogen around the beam with thermal deuterons. The created thermal neutrals again can be excited by collisions or undergo further charge exchange reactions with impurity atoms.

Near the wall recombined plasma particles can produce a dense neutral particle population that does charge exchange with plasma ions. This is referred to as passive charge exchange or Luke warm component in the spectrum.

The plasma background radiation and the passive charge exchange can be discriminated by a chopped diagnostic beam. Using instead of hydrogen other elements (Li, He) also the halo effect does not appear. In fig. 6 the spectrum of a CVI CXR-line is shown, which is obtained by a hydrogen diagnostic beam injected into an ohmic discharge at TEXTOR at the last closed magnetic surface. Only one Gaussian fit was necessary to describe the measured profile. The apparent ion temperature of 317 eV deduced from the FWHM was corrected to a true ion temperature of 277 eV.

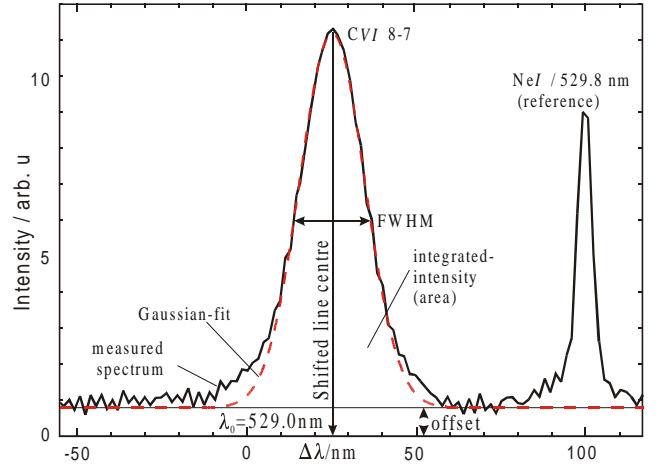


Figure 6: Spectral profile of  $C^{5+}$  charge exchange recombination line measured with the 50 keV H diagnostic beam at TEXTOR

## IV. ATOMIC BEAM SOURCES

### IV.1. Thermal Li-beam

Thermal Li-beams firstly have been applied for the determination of electron density profiles with particle beams. Li is chosen because the excitation- and ionisation rate coefficients show only a weak dependence on  $T_e$  in the range from 10 eV to 150 eV. In equation 6 they can be set constant and be written in a simplified form.

$$n_e = \frac{\overline{v_{Li}} I_{Li}(r)}{\langle \sigma_I v_e \rangle \int_0^r I_{Li}(r') dr'} \quad (11)$$

As can be seen from equation 11 the whole emission profile of the strong transition  $2p \rightarrow 2s$  at 670.8 nm must be observed in order to allow an integration from inside the plasma which corresponds to the density of the neutral Li-atoms at the position  $r$ . Then no other calibration is necessary to evaluate the electron density profiles. The velocity is given by the temperature of the oven and a rate coefficient for ionisation of  $9 \cdot 10^{-13} \text{ m}^3/\text{s}$  at 30eV usually is chosen.

Initially pure lithium was filled in an oven and heated up to  $600^\circ\text{C}$ . The Li-flux (partial pressure  $\approx 1 \text{ mb}$ ) was so high that the source could be placed in about 1 m distance from the plasma. But the liquid Li was difficult to handle and also the rise of a solid  $\text{Li}_2\text{O}$  and  $\text{LiH}_2$  layer reduced the reliability of the source.

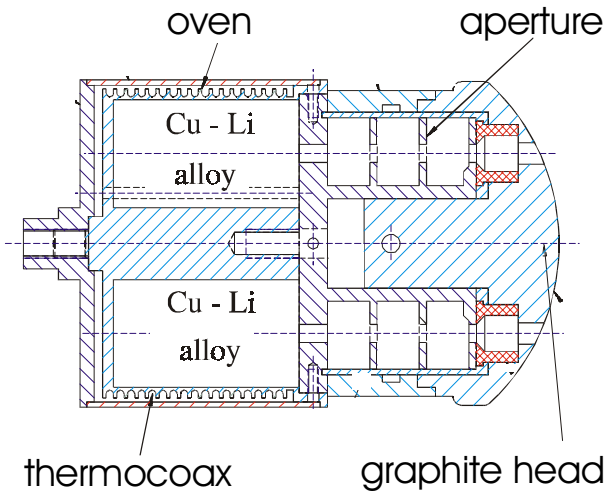


Figure 6: Cut through a double beam thermal Li oven used for fluctuation measurement of  $n_e$

The application of Al/Li (melting point  $604^\circ\text{C}$ ) or Cu/Li (melting point  $1000^\circ\text{C}$ ) alloys, which have strong diffusion of Li atoms to the surface<sup>17</sup>, did allow to build reliable and in any direction mountable sources with long operational times ( $>500 \text{ h}$ ). A cut through an oven used for fluctuation measurements with 2 beams is shown in fig. 6. The housing of the oven is made of stainless steel heated by a thermocoax. For every beam two pieces of a Cu/Li-alloy, one with a hole of 5 mm are inserted. Apertures determine the beam divergence. Cu/Li alloy at a temperature of  $700^\circ\text{C}$  deliver flux densities of  $5 \cdot 10^{18}/\text{m}^2\text{s}$  in a distance of 100 mm from the source, which is the typical distance to the measurement volume. The corresponding velocity of the Li-atoms is 1.7 km/s so that a density of  $3 \cdot 10^{15}/\text{m}^3$  is possible. This value is more than a factor of 100 below the measured electron density in the plasma edge. But the source must be located near the plasma edge to reach sufficient high Li-densities.

In fig. 7 the line emission profile of Li in a discharge of TEXTOR and the corresponding  $n_e$ -profile is presented. The data have been recorded with a linear diode array of

128 pixels. The time resolution was 20 ms. The penetration depth is  $2.4 \cdot 10^{16}/\text{m}^2$  and can be deduced from the product of the ionisation length  $\lambda_i$  and  $n_e$ . Densities below  $4 \cdot 10^{18}/\text{m}^3$  are measured reliable. Above that the population of higher states and changes in the mean velocity have to be taken into account. The double Li-beam has been applied for the simultaneous measurement of radial and poloidal  $n_e$ -fluctuations. For parameter in the plasma edge of TEXTOR thermal Li has a relaxation time of  $0.2 \mu\text{s}$ . At a sampling rate of 500kHz the electron density is always measured under stationary conditions of the population distribution.

Thermal Li-beams have also applied in low temperature plasmas. In such plasmas with electron temperatures below 5 eV, the rate coefficients for excitation and ionisation are not constant anymore. It could be shown that the ratio of rate coefficients into different states shows temperature dependence. The line intensity ratio of two transitions ( $3d \rightarrow 2p$  and  $2p \rightarrow 2s$ ) is observed, which allows the determination of the electron temperature, if the electron density is known. This in some cases can be deduced from the previous method if the Li-beam is fully ionised. This method can be applied if the gas pressure is below 0.01mb. Otherwise the mean free path of Li-atoms in the gas is too low and the elastic scattering with the neutral gas stops the beam<sup>18</sup>.

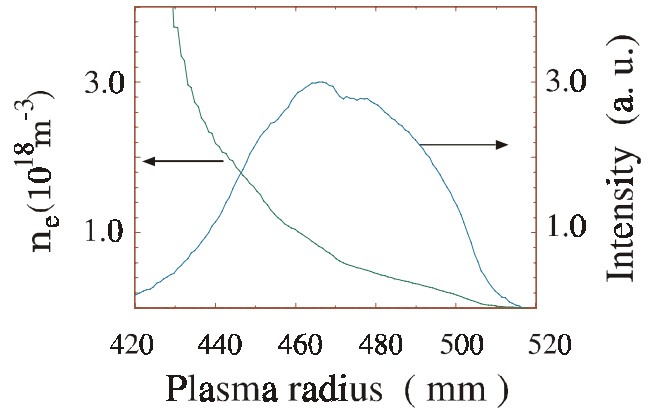


Figure 6: Radial line emission profile of Li and corresponding  $n_e$ -profile in TEXTOR

#### IV.2. Thermal He-beam

Thermal He-beams are applied for the simultaneous measurement of  $n_e$  and  $T_e$  profiles in the plasma edge. The line intensity ratios of the transitions  $3^1\text{D} \rightarrow 2^1\text{P}$  ( $\lambda_1=667.8 \text{ nm}$ ) and  $3^1\text{S} \rightarrow 2^1\text{P}$  ( $\lambda_2=728.1 \text{ nm}$ ), respectively  $3^1\text{S} \rightarrow 2^1\text{P}$  and  $3^3\text{S} \rightarrow 2^3\text{P}$  ( $\lambda_3=706.5 \text{ nm}$ ) are calculated for a local position inside the plasma edge and compared with the values obtained from a collisional-radiative model, shown in fig. 4.

The He effusive source consists of a collimating hole structure. A tube with 8 mm diameter and  $l=35 \text{ mm}$  length is filled with small tubes with  $2r=0.2 \text{ mm}$  inner diameter and 0.1 mm wall thickness.

Brix has given the relation for the particle flux of a long tube effusive source<sup>19</sup>.

$$\dot{N}_{effusion} = \frac{2r}{3l} n_{He} \overline{v_{He}} A \quad (12)$$

where  $n_{He}$  = density of He at the reservoir and  $v_{He}=1.6$  km/s at 200°C. The reservoir of  $2 \cdot 10^{-3} \text{ m}^3$  is filled with 10mb He. The resulting flux is  $2 \cdot 10^{18}/\text{s}$ . With  $\pm 20^\circ$  the beam divergence is quite large so that in a distance of 100 mm a He-beam density of  $9 \cdot 10^{16}/\text{m}^3$  is received. In fig. 8 the line emission profiles of all three transitions observed in a TEXTOR discharge and the corresponding  $n_e$  and  $T_e$

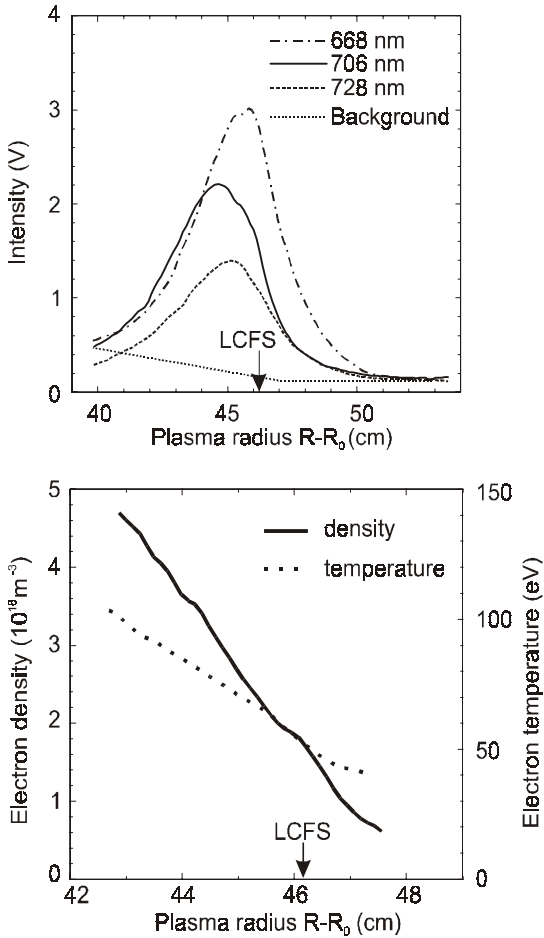


Figure 8: Measured radial line emission profiles of He and corresponding  $n_e$  and  $T_e$  profiles in TEXTOR

profiles are presented. The profiles can be measured quasi-continuously with a time resolution of 1 ms. Due to the high divergence this source cannot be used for fluctuation measurements. This would be possible with a supersonic He-beam.

#### IV.3. Supersonic He-beam

He gas of high pressure (10 to 70 bar) is passing an aperture with  $40\mu\text{m}$  diameter and can expand into a vacuum of  $<10^{-3}$  mb. The velocity is about 20% larger than in

an effusive source. As a consequence of the adiabatic expansion of the beam the temperature drops, which leads to a reduction of the velocity distribution. Nearly monoenergetic He beams are established. The central part of the beam is cut out by a skimmer with  $200\mu\text{m}$  diameter, located about 10 mm from the nozzle (fig. 9).

This determines the beam divergence. In TEXTOR a beam divergence of  $\pm 1^\circ$  was established. The pressure in the expansion chamber must be maintained below  $10^{-3}$  mb otherwise the beam will break down. The pumping capacity is limiting the He-flux in TEXTOR to only  $3 \cdot 10^{17}/\text{s}$ <sup>20</sup>. But this should be sufficient for fluctuation measurements on  $T_e$  and  $n_e$ . The data evolution of the emission signals is identical with that for effusive sources.

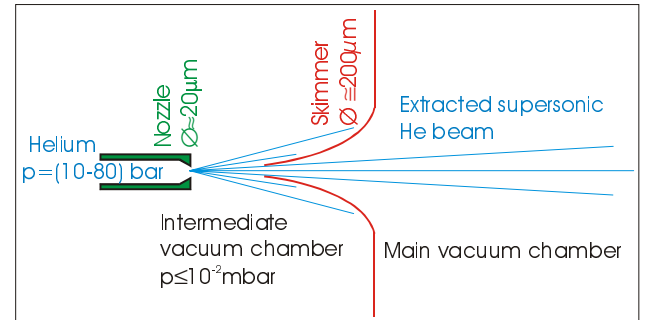


Figure 9: Schematic arrangement of the supersonic He-beam diagnostic

#### IV.4. Laser blow-off

Particles with energies of a few eV are produced by evaporation by means of powerful laser radiation ( $>10\text{MW}$ ), which can fill the gap between the ion beams (keV) and thermal sources (0.1 eV). The blow-off system (ablation system) consists of a glass or quartz substrate, which is coated either by a single species or a multilayer of different materials of several 100 nm thickness. The layer must absorb the laser radiation that enters through the rear side. It has been observed that the velocity of the different species is identical. Atoms, ions and clusters are released from the target that is about 1 m far from the observation volume. By the difference of speed the suprathreshold particles are discriminated from the clusters, which are much slower. The ions are deflected by the magnetic field. Slight variations of the energy and flux density are possible by changing the spot size. A Ruby laser, which allows only single shot operation (1 shot /min) has first been applied<sup>21</sup>. At TEXTOR multi layer targets with Cr, LiF and C are used for the measurement of  $n_e$  and  $T_e$  profiles. The penetration depth is  $1 \cdot 10^{17}/\text{m}^2$ . Easily all condensed materials (micro pellets<sup>22</sup>) can be injected into the plasma by laser blow-off, which is done for transport investigations. Nowadays NdYAG ( $\lambda=1024$  nm) and XeCl excimer laser ( $\lambda=308\text{nm}$ ) have been introduced with repetition rates up to 20 Hz. They need fast moving targets. At TEXTOR and W7-AS a system with 15 targets of each 50 mm square can be inserted in the vacuum system.

#### IV.5. Ion source

The most complex atomic beam systems are neutralised ion beams. Mainly they are used for the measurement of  $n_{\text{imp}}$ ,  $T_{\text{imp}}$  and rotational velocities observing charge exchange recombination lines. A wide selection of ion sources is applied. Plasmas discharges are produced by means of hot filaments, radio frequency (rf) or microwave (ECR) heating. For gases, which can form molecules, the heating method and the wall conditions of the containment determine the molecular ion fractions ( $\text{H}^+$ ,  $\text{H}_2^+$ ,  $\text{H}_3^+$ ). The ions are subtracted from the plasma by an ion optical, 3 or 4 grids, system. In fig. 10 the experimental arrangement of a 50 keV H diagnostic beam at TEXTOR is shown<sup>23</sup>.

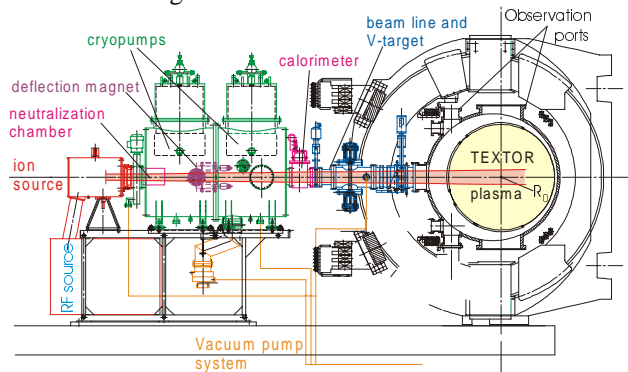


Figure 10: 50 keV H diagnostic beam at TEXTOR

The temperature of the beam plasma and the acceleration voltage mainly determine the divergence that should be below  $\pm 0.6^\circ$  in order to maintain sufficient particle flux into the plasma. The ion beam has to cross a neutraliser cell where the fast ions capture an electron by charge exchange reactions. Here an optimum in the gas pressure has to be established where a maximum of neutralisation is reached with an acceptable attenuation of the beam. The molecule ions are also neutralised but they have correspondingly lower energies. This can disturb the measurement especially in the plasma edge. The surviving ions are deflected to a beam dump by magnetic forces. For diagnostic purposes it should be possible to chop the plasma source and the acceleration voltage. The penetration depth is dependent on the energy of the beam atoms. The cross-section for the CXR of H-atoms reaches a maximum value at about 50 keV. In high-density plasmas this energy might be too low to reach the plasma centre.

A special solid-state source for Li ions is applied at several experiments<sup>24</sup>. A  $\beta$ -eucryptite emitter is heated up to 1300°C. If a voltage is applied surface ionisation occurs and Li-ions are extracted, which are neutralised in Li or Na vapour. This source is reliable and can be used for CXRS and also for the determination of  $n_e$  profiles. The Li current is dependent on the voltage and the size of the emitter.

<sup>1</sup> A. Unsöld, „Physik der Sternatmosphären“, Springer Verlag Berlin (1955)

<sup>2</sup> F. Meijer, “Plasma Spectroscopy”, Transaction Fusion Techn. **37** Mar. 2000 352-359

<sup>3</sup> A. Pospieszczyk, “Diagnostics of Edge Plasmas by Optical Methods”, *Atomic and Plasma-Material Interaction Processes In Controlled Thermonuclear*, R.V. Janev and H.W. Drawin, p 213 ELSEVIER, Caderache, (1993)

<sup>4</sup> C.J. Barth, “Laser-Aided-Plasma-Diagnostic” Transaction Fusion Sci. Techn. **41** Mar. 2002 386-393

<sup>5</sup> A.A.E. Van Blokland, “Ion Temperature Measurements in Tokamak Plasmas by Rutherford Scattering” PhD thesis, Utrecht University (1991)

<sup>6</sup> Ph. Mertens, A. Pospieszczyk, J. Nucl. Mat. **266-269** (1999) 884-889

<sup>7</sup> M. Brix “Calculation of the Penetration Depth and Line Emissions of Energetic Helium Beam”, Jül-3638 (1998)

<sup>8</sup> A. Huber, A.V. nedospasov, U. Samm, B. Schweer, J. Nucl. mat. **266-269** (1999) 546-551

<sup>9</sup> N. Brenning 1980 J. Quant. Spectrosc. Radiation Transfer **24** 1173

<sup>10</sup> V.A. Abramov, L.A. Vainstein, “Recommended cross-section and rates for electron inelastic collisions with helium”, I.V. Kurchatov Institute, Moskau, (1987)

<sup>11</sup> B. Brosda, Dissertation, Ruhr-Uni Bochum (1993)

<sup>12</sup> B. Schweer, G. Mank, A. Pospieszczyk, B. Brosda, B. Pohlmeier, J. Nucl. Mater. **196-198** (1992) 174

<sup>13</sup> M. Brix, , „Messung von Elektronentemperatur und – dichte mittels Heliumstrahldiagnostik im Randschicht-plasma eines Tokamaks“, Jül-3638, (1998)

<sup>14</sup> M.G. von Hellermann and H.P. Summers *Active Beam Spectroscopy in JET in Atomic and Plasma-Material Interaction Processes in Controlled Thermonuclear Fusion*, Ed. R. V. Janev and H W Drawin, Elsevier Science Publishing, (1993), p142-145

<sup>15</sup> E. Hintz, B. Schweer, Plasma Phys. Control. Fusion **37** (1995), A87

<sup>16</sup> A. Maas, “Helium distribution functions in tokamak plasmas”, thesis, Utrecht University (1995)

<sup>17</sup> R.P. Schorn, „Untersuchungen zur Zerstäubung von Kupfer/Lithium-Legierungen“, JÜI-2367, (1990)

<sup>18</sup> A. Beck, D. Hemmers, H. Kempkens, B. Schweer, J. Uhlenbusch, J. Phys. D: Appl. Phys. **33** (2000) 360-366

<sup>19</sup> M. Brix, B. Schweer, 24<sup>th</sup> EPS-Conference on Controlled Fusion and Plasma Physics, (1997), 1837

<sup>20</sup> U. Kruezi, “Entwicklung eines modulierbaren Helium Überschallstrahls zur Messung von Fluktuationen der Elektronentemperatur und –dichte“, FZJ Internal Report (2002)

<sup>21</sup> A. Pospieszczyk, G.G. Ross, Rev. Sci. Instrum. **59** (4), (1988), 605

<sup>22</sup> S. Zoletnik, G. Kocsis et al., Rev. Sci. Instrum., **66** (1995) 2904

<sup>23</sup> A.A. Ivanov, V.I. Davydenko, P.P. Deichuli et al. Review Sci. Instr. **71** no. 10 (2000) 3728-3735

<sup>24</sup> S. Fiedler, R. Brandenburg et al. J. Nucl. Mat. **266-269** (1999) 1279